Effect of different wastewater composition on kinetics, capacities, and mechanisms of phosphorus sorption by carbonated bauxite residue

Cristian Barca, Matteo Magari, Hélène Miche, Pierre Hennebert

Effect of different wastewater composition on kinetics, capacities, and mechanisms of phosphorus sorption by carbonated bauxite residue

Cristian Barca [a,*], Matteo Magari [a,b], Hélène Miche [c], Pierre Hennebert [d]

[a] Aix-Marseille Univ., CNRS, Centrale Marseille, M2P2 UMR 7340, Marseille, France
[b] Department of Civil-Environmental Engineering and Architecture (DICAAR), University of Cagliari, Via Marengo 2, 09123 Cagliari, Italy
[c] Aix-Marseille Univ., CNRS, IRD, INRAE, Collège de France, UM 34 CEREGE, Aix en Provence, France
[d] INERIS, BP 2, F-60550 Verneuil-en-Halatte, France

ARTICLE INFO

Editor: Chao He

Keywords:
Wastewater treatment
Phosphate adsorption
Phosphate precipitation
Bauxite residue
Kinetic study

ABSTRACT

This study aims at evaluating the effect of different wastewater composition on kinetics, capacities, and mechanisms of P sorption by carbonated bauxite residues (CBR). A series of batch experiments was performed to investigate P sorption behaviors from solutions prepared with different aqueous matrices (deionized water, tap water, and real wastewater) and different initial P concentrations (from 10 to 200 mg P/L). Also, a series of sequential P extractions was performed to investigate P fractionation of CBR before and after its use in P sorption experiments, and hence to elucidate the main P removal mechanisms. The results indicate that initial P concentration is the most influential parameter controlling kinetics, capacities, and mechanisms of P removal in batch experiments. Kinetic constant of P sorption increases exponentially with decreasing initial P concentration below 100 mg P/L, thus indicating a faster achievement of P sorption equilibrium. Equilibrium P sorption capacities increase linearly from about 0.2 to about 3.9 mg P/g CBR with increasing initial P concentration from 10 to 200 mg P/L, thus indicating that P saturation of CBR was not reached. Ca phosphate precipitation is the main P removal mechanism at higher initial P concentrations (> 10 mg P/L), whereas phosphate adsorption on CBR surface becomes more relevant over the total amount of P removed at lower initial P concentrations. Overall, the findings of this study allow to evaluate kinetic constants, sorption capacities, and removal mechanisms under different operating scenarios, thus providing crucial information for the design and operation of P treatment units.

1. Introduction

Bauxite residue is a Fe and Al oxide-rich waste produced in large amounts by the aluminum industry (world production about 200 Mt in 2018) [1], of which no more than 3–5% is reused in a productive way (e.g. cement and ceramic production) [2]. Therefore, the accumulation of bauxite residues in storage sites is becoming an increasingly serious problem, and the identification of sustainable ways of valorization is a topical issue for researchers and professionals in the field of waste management [3].

During the last two decades, several researchers have investigated the application of bauxite residue as material for environmental remediation, including wastewater treatment, gas treatment, and soil remediation [4]. Among the different applications, the use of bauxite residue as sorbent material to remove phosphorus (P) from wastewater has received increasing attention in recent years [5–8]. The main objective of these studies was to develop low cost P treatment solutions, especially for small wastewater treatment plants (WWTPs) [9]. Bauxite residue has a high alkaline nature [3] and it can produce high pH leachates (up to 13) when used for environmental applications [2]. Therefore, bauxite residue pretreatments with gypsum, seawater, or acids (H_2SO_4, HCl, HNO_3, and H_3PO_4) are proposed in the literature to neutralize its alkalinity and reduce pH leachates below 9 [1]. According to the literature, maximum P removal capacities range from 6 to up than 33 mg P/g bauxite residue [10,11], thus depending on the type and composition of bauxite residue and on the experimental parameters established for the experiments. A large variety of P removal mechanisms are described in the literature, including physical, electrostatic, and chemical adsorption, and Ca phosphate precipitation [12–14]. However, most of the studies were performed using very simple synthetic P solutions, which

* Corresponding author.
E-mail address: cristian.barca@univ-amu.fr (C. Barca).

did not contain all the components occurring in real effluents that may affect P sorption (e.g. competing anions such as nitrate, carbonate, and sulfate) [15,16]. To the best of our knowledge, only a few studies have investigated the P removal performances of bauxite residue by using real effluents [17,18], and the effect of different wastewater composition on P sorption behavior has not yet been fully elucidated.

This study aims at evaluating the effect of different wastewater composition on kinetics, capacities, and mechanisms of P sorption by carbonated bauxite residue (CBR). A series of batch experiments was performed to investigate P sorption behaviors from solutions prepared with five different aqueous matrices (deionized water, deionized water plus nitrate, tap water, tap water plus nitrate, and real wastewater) and four different initial P concentrations (10, 50, 100, and 200 mg P/L). Also, a series of sequential P extractions was performed to investigate the P fractionation of CBR before and after its use in P sorption experiments, and hence to elucidate the main P removal mechanisms.

The novelty and importance of this paper are highlighted by the following two points:

(i) A comprehensive batch study investigating the effect of different wastewater composition on P sorption behaviors of CBR. The use of the same experimental procedure allows to compare the influence of different aqueous matrices and initial P concentrations on kinetics and capacities of P sorption.
(ii) An in-depth critical investigation of the P removal mechanisms achieved by CBR. A systemic approach, involving the integration and analysis of experimental results from P sorption and chemical extraction experiments, was followed to investigate the influence of different aqueous matrices and initial P concentrations on P removal mechanisms.

Overall, the results of this study provide crucial information for the design and operation of P treatment units that use CBR as sorbent material, as they allow to estimate kinetic constants, sorption capacities, and removal mechanisms under different operating scenarios.

2. Material and methods

2.1. Bauxite residue collection and preparation

The samples of bauxite residue used in this study were provided by the company ALTEO (Gardanne, France). They were obtained through solid separation from the effluents of the Bayer process in a filter press, and their main chemical composition was Fe_2O_3 (45–53%), Al_2O_3 (10–16%), TiO_2 (9–15%), SiO_2 (5–8%), CaO (3–8%), and Na_2O (3–5%) (data from ALTEO). Before P sorption experiments, bauxite residue was treated with gypsum at a dried mass ratio of 5% (mass of gypsum to mass of bauxite residue). Then the mixture was turned approximately twice a day for 4 days in order to improve the contact of the material with atmospheric CO_2 and thus produce carbonated bauxite residue (CBR), according to Eq. (1). This was done to neutralize the NaOH content and decrease the pH of CBR leachates below a value of 9, as described by Cusack et al. [19].

$$2NaOH + CaSO_4 \bullet 2H_2O + CO_2 \rightarrow CaCO_3 + Na_2SO_4 + 3H_2O \quad (1)$$

After carbonation, CBR was sieved and the fraction less than 2 mm was collected to perform batch experiments. Water content of CBR was determined after heating at 105 °C until constant weight.

2.2. P sorption experiments

A series of batch experiments was performed to investigate the effect of different water composition on kinetics and capacities of P sorption. Five aqueous matrices were considered: (i) deionized water, (ii) deionized water plus 40 mg $N\text{-}NO_3$/L, (iii) tap water, (iv) tap water plus 40 mg $N\text{-}NO_3$/L, and (v) real effluent from a small WWTP (a two vertical flow constructed wetland treating the domestic wastewater of about 1500 people equivalent, Rougiers, France). Aqueous matrices (ii) and (iv) were prepared by adding KNO_3 to deionized and to tap water, respectively, this to simulate common nitrate ($N\text{-}NO_3$) concentration of small WWTP in France (56 ± 25 mg $N\text{-}NO_3$/L, average values ± standard deviations of 151 plants) [20]. Table S1 (Supplementary Information) summarizes the main chemical composition of tap water and real effluent used for batch experiments.

For each aqueous matrix, four P solutions at different initial P concentrations (10, 50, 100 and 200 mg P/L) were prepared by dissolving different masses of KH_2PO_4. Each batch test was performed at a liquid to solid ratio of 20 L/kg (ASTM D 4646), by adding 35 g of CBR (mass dry equivalent) into a 1 L plastic bottle containing 0.7 L of P solution. Then, the bottles were rotary agitated at 5 r/min (rotary agitator STR4, Stuart, UK) under room temperature (20 ± 1 °C), and aqueous samples were collected from each bottle after 0.5, 1, 2, 4, and 6 h. The aqueous samples were filtrated with a 0.45 μm filter before P analysis.

For each series of experiments, experimental P sorption capacities q_t (mg P/g CBR) were determined by Eq. (2), where $_{Pi}$ and P_t are the P concentrations at initial time and at time t, respectively, V is the solution volume (L), and m is the dried mass equivalent of CBR (g).

$$q_t = \frac{(P_i - P_t) \bullet V}{m} \quad (2)$$

Experimental sorption capacities q_t were then modeled using the integrated forms of the pseudo first order kinetic Eq. (3) and the pseudo second order kinetic Eq. (4) [21]. In Eqs. (3) and (4), q_{e1} and q_{e2} are the sorption capacities at the equilibrium for the pseudo first and the pseudo second order, respectively (mg/g), t is time (h), k_1 and k_2 are the constant rates of the pseudo first (1/h) and the pseudo second order (g/(mg•h)), respectively. The equilibrium capacity q_{e1} must be known to exploit Eq. (3) with experimental data. In this study, q_{e1} was considered an adjustable parameter whose value was estimated by trial and error until the difference between the values of q_{e1}-trial and q_{e1} calculated by Eq. (3) was less than 0.1%.

$$\ln(q_{e1} - q_t) = lnq_{e1} - k_1 \bullet t \quad (3)$$

$$\frac{t}{q_t} = \frac{1}{k_2 \bullet q_{e2}^2} + \frac{1}{q_{e2}} \bullet t \quad (4)$$

2.3. Chemical extractions

A series of supplementary batch experiments and chemical extractions were performed to investigate the effect of different water composition on P removal mechanisms. Four P solutions were prepared by adding different masses of KH_2PO_4 to deionized water and real effluent from a small WWTP (Rougiers, France): deionized water at around 10 mg P/L (test 10 H_2O), deionized water at around 100 mg P/L (test 100 H_2O), real effluent at around 10 mg P/L (test 10 WW), and real effluent at around 100 mg P/L (test 100 WW). For each test, 1 g of CBR (mass dry equivalent) was put into a 30 mL plastic centrifuge tube containing 20 mL of P solution, thus according to a liquid to solid ratio of 20 L/kg (ASTM D 4646). Then, the tubes were rotary agitated at 5 r/min under room temperature (20 ± 1 °C). After 24 h of agitation, supernatants and CBR pellets were separated by centrifugation at 8000 g for 20 min. The supernatants were filtrated with a 0.45 μm filter before pH measures and P, Ca, Al, and Fe analyses, whereas the CBR pellets were used to perform chemical extractions.

A three-step sequential extraction, adapted from Standards, Measurements and Testing protocol (STM) [22] and from the modified Hedley fractionation protocol (according to Tiessen and Moir [23,24]), was followed to sequentially extract three different P fractions from each CBR pellet (Fig. S1, Supplementary Information):

i. Step 1: Non-apatite inorganic P (NAI-P) was extracted in 20 mL of 1 M NaOH. This fraction is primarily related to phosphates that can be desorbed from CBR by OH^- exchange and/or P bound to Al and/or Fe compounds that are soluble at high pH.
ii. Step 2: Apatite inorganic P (AI-P) was extracted in 20 mL of 1 M HCl. This fraction is defined as Ca bound P, as P extraction in this step is mainly due to dissolution of Ca-P complexes at low pH.
iii. Step 3: Residual P (RES-P) was extracted in 12 mL of concentrated HCl (about 10 M) in a 20 min water bath at 80 °C. This fraction represents P in stable compounds that need much more energy to be dissolved.

The fractions (i) and (ii) were determined after 16 h of rotary agitation at 5 r/min at room temperature. After each extraction, supernatants and CBR pellets were separated by centrifugation at 8000 g for 20 min. Then, the supernatants from each extraction were filtered (0.45 µm filters) before P, Ca, Al, and Fe analyses. This three-step extraction protocol has also been applied to raw CBR, with the aim of quantifying the P fractions in CBR before its use for wastewater treatment, and to CBR after 140 days of continuous flow P sorption experiments (Column A in Barca et al. [25]), with the aim of investigating P removal mechanisms of CBR under continuous flow conditions. All the supplementary batch experiments and chemical extractions were performed in duplicate.

2.4. Analytical methods

The pH values of the aqueous samples were measured using a multiparameter analyzer Consort C5020 (Turnhout, Belgium). P analyses were performed according to the ammonium molybdate spectrometric method (EN ISO6878, 2004) by a spectrophotometer WTW PhotoLab 6600 UV–VIS (Weilheim in Oberbayern, Germany). Elemental analyses

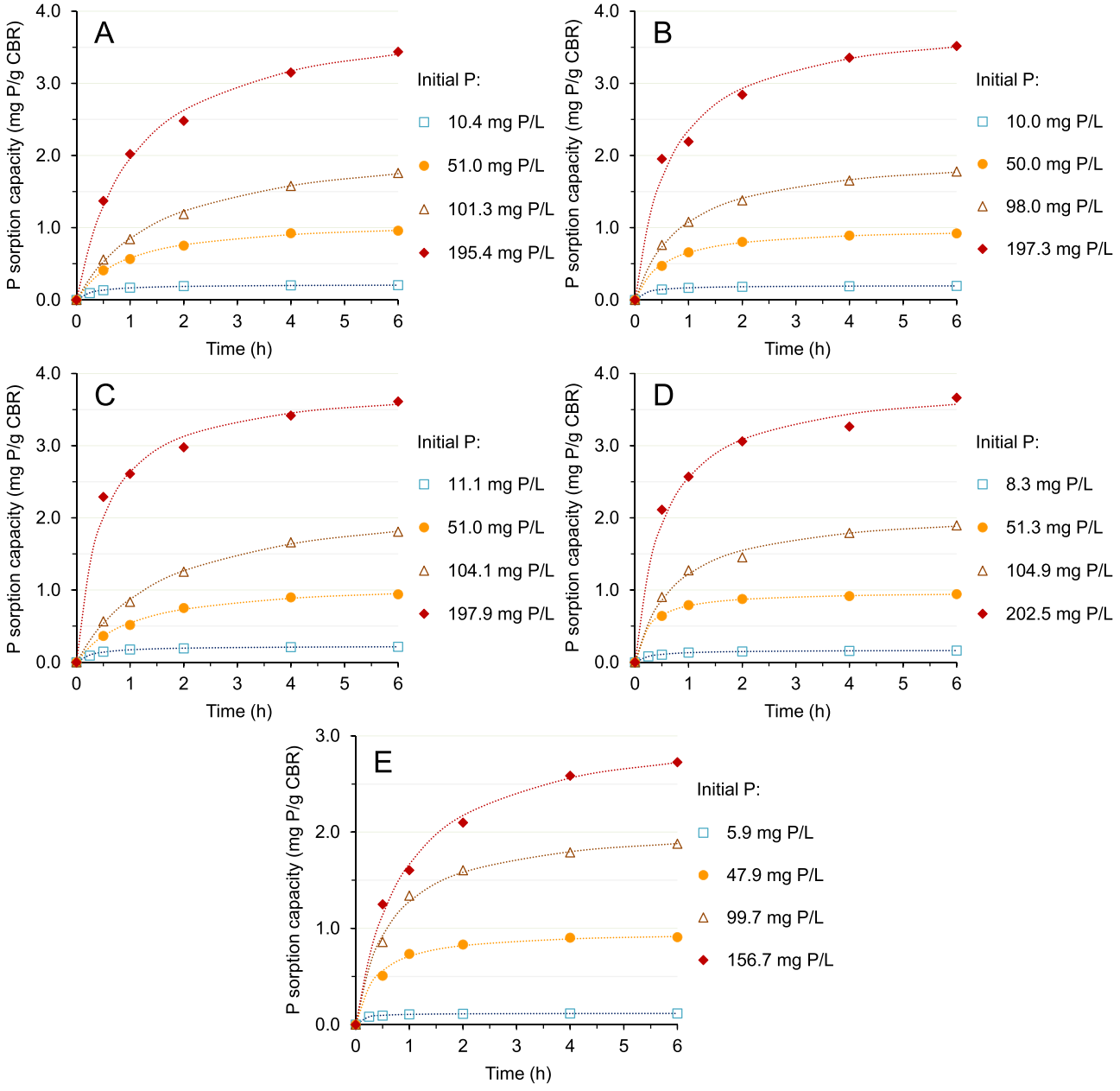

Fig. 1. Experimental P sorption capacities as a function of time for the experiments performed at different initial P concentrations and different aqueous matrices: (A) deionized water; (B) deionized water plus 40 mg $N\text{-}NO_3$/L; (C) tap water; (D) tap water plus 40 mg $N\text{-}NO_3$/L; (E) real effluent from a WWTP. Dotted curves show the modeled P sorption capacities using the pseudo second order kinetic equation.

(Al, Ca, and Fe) were performed by inductively coupled plasma atomic emission spectroscopy (ICP-AES) using a spectrometer Jobin Yvon Horiba Ultima-C (Horiba, Japan). For each set of analyses, limit of detection and limit of quantification were determined by analysis of blanks. All chemicals used were of analytical grade.

3. Results and discussion

3.1. P sorption kinetics

The evolutions of experimental P sorption capacities as a function of time for the experiments performed with different aqueous matrices and different initial P concentrations are summarized in Fig. 1. The pseudo equilibrium on P sorption was achieved after 6 h of contact time for all experiments, with the pseudo equilibrium reached faster as the initial P concentration decreases. As shown in Table 1, the correlation coefficients R^2 of the pseudo second order model were higher than those of the pseudo first order model for all experiments. Pseudo first and pseudo second order models have mostly be considered empirical, but according to several authors there could be a link of these models to the physical-chemical nature of the adsorption process [26,27]. On the one hand, the pseudo first order model is often more suitable for describing simple mono-type adsorption processes which primarily depend on the availability of adsorption sites on the adsorbent surface, as it can graphically describe the rapid initial rise of the sorption capacity over time and the fast achievement of equilibrium as soon as the adsorption sites are saturated [26,28]. On the other hand, the pseudo second order is often more suitable for describing processes in which the removal of pollutants is governed by a mix of different mechanisms, including adsorption and chemical reactions such as precipitation, with the concentration of one or more reactants controlling the rate of the process [21,26]. According to this, the higher R^2 values of the pseudo second order may indicate that P sorption on CBR is due to a mix of removal mechanisms such as physical, and/or electrostatic, and/or chemical adsorption, but also chemical precipitation, as already suggested by previous studies [10,29].

For all aqueous matrices tested in this study, the kinetic constant of the pseudo second order model k_2 increases exponentially with decreasing initial P concentrations below a value of 100 mg P/L (Fig. 2A), thus indicating a faster achievement of sorption equilibrium at a lower initial P concentration. This behavior suggests that sorption mechanisms vary according to the value of initial P concentration. Most probably, phosphate adsorption on CBR surface was more relevant at lower initial P concentration, whereas chemical precipitation becomes more relevant at higher initial P concentration, when adsorption sites on CBR surface are more quickly saturated. This hypothesis appears to be confirmed by the findings of recent studies [8,29], which indicate that physical adsorption of phosphates has a significant impact on P sorption capacities under P concentrations lower than 10 mg P/L [8] whereas P precipitation becomes more relevant as the initial P concentration increases [29].

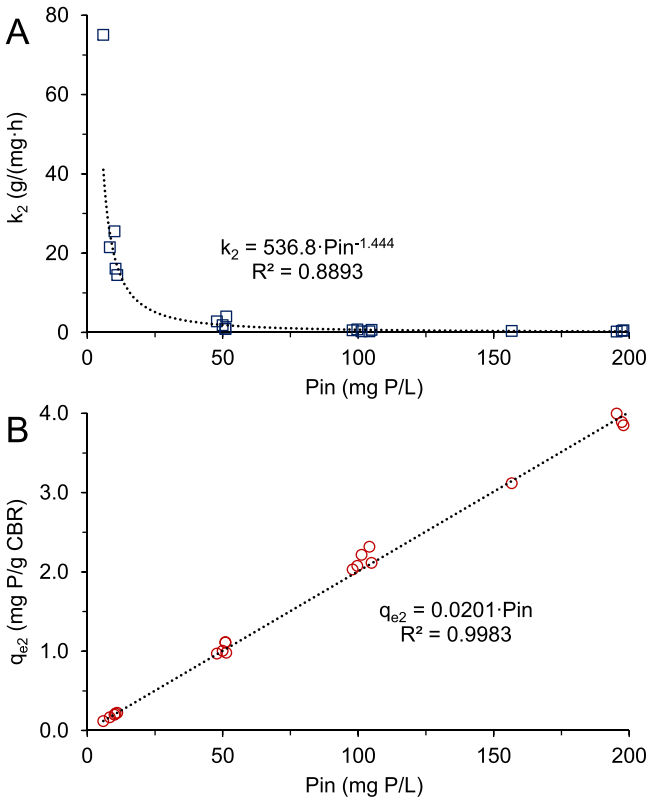

Fig. 2. Main results of modeling P sorption capacities according to the pseudo second order kinetic model: (A) kinetic constant k_2 as a function of initial P concentration Pin; (B) equilibrium sorption capacity q_{e2} as a function of initial P concentration Pin.

Fig. 2B shows a very good linear correlation between the equilibrium

Table 1
Main results of modeling experimental P sorption capacities by using the pseudo first and the pseudo second order kinetic models.

Aqueous matrix	Initial P (mg P/L)	Pseudo first order model			Pseudo second order model		
		q_{e1} (mg P/g CBR)	k_1 (1/h))	R^2 (-)	q_{e2} (mg P/g CBR)	k_2 (g/ (mg • h))	R^2 (-)
Deionized water	10.4	0.20	1.484	0.9120	0.22	16.087	0.9998
	51.0	0.96	0.839	0.9940	1.11	0.989	0.999
	101.3	1.81	0.571	0.9872	2.22	0.281	0.9983
	195.4	3.47	0.712	0.9633	3.99	0.240	0.9977
Deionized water + 40 mg N-NO_3/L	10.0	0.19	1.536	0.8697	0.20	25.517	1.0000
	50.0	1.32	0.128	0.8373	1.01	1.858	0.9999
	98.0	1.78	0.783	0.9601	2.03	0.557	0.9996
	197.3	3.53	0.925	0.9552	3.89	0.392	0.9977
Tap water	11.1	0.21	1.374	0.8882	0.22	14.484	0.9997
	51.0	0.95	0.792	0.9947	1.12	0.854	0.9984
	104.1	1.86	0.587	0.9963	2.32	0.261	0.9986
	197.9	3.62	1.039	0.8913	3.85	0.564	0.9982
Tap water + 40 mg N-NO_3/L	8.3	0.16	1.422	0.8774	0.17	21.482	0.9999
	51.3	0.94	1.386	0.8646	0.98	4.010	0.9999
	104.9	1.90	0.864	0.9523	2.12	0.646	0.9979
	202.5	3.67	0.940	0.8357	3.88	0.498	0.9956
Real effluent from a WWTP	5.9	0.12	2.615	0.9474	0.12	75.083	1.0000
	47.9	0.91	1.514	0.9738	0.97	2.780	0.9992
	99.7	1.88	0.975	0.9414	2.08	0.771	0.9993
	156.7	2.74	0.811	0.9784	3.12	0.368	0.9984

sorption capacity for the pseudo second order model q_{e2} and the initial P concentration Pin (Eq. (5)), as indicated by the high value of R^2 (0.9983).

$$q_{e2} = 0.0201 \bullet Pin \quad (5)$$

This indicates that P saturation capacity of CBR was not achieved, and equilibrium sorption capacities increase linearly by increasing the initial P concentration over the full range of values that have been tested (from 10 to 200 mg P/L). Moreover, the results in Fig. 2B clearly confirm that the different aqueous matrices used in this study did not significantly affect P sorption capacity, but the main parameter influencing P sorption in batch experiments was the initial P concentration.

The results of this study are compared to those of recent batch studies that have investigated P sorption kinetics of raw and modified bauxite residue (Table 2). As shown in Table 2, most studies were performed by using very simple synthetic solutions often prepared by dissolving phosphate salts (e.g. KH_2PO_4) in deionized water. It should be also noticed that it is difficult to compare the results of the different studies because of the large discrepancy between the experimental parameters that were established for the batch experiments. According to data in Table 2, P sorption on bauxite residue appears to be a relatively fast process, as usually a pseudo equilibrium in P sorption is achieved within 12 h of contact time. Overall, experimental P sorption capacities vary from 0.1 to 33 mg P/g of bauxite residue, and they appear to increase with increasing the initial P concentration from 5 to 200 mg P/L and/or with decreasing the sorbent dose from 50 to 0.1 g/L (Table 2). Modified bauxite residue often shows better P sorption performance than raw bauxite residue. According to Park et al. [29], thermal treated bauxite residue (brown mud, as described by Kaußen and Friedrich [30]) can give P sorption capacities 2.3 times higher than raw bauxite residue, probably because thermal activation enhanced the surface density of adsorption sites [13]. Wang et al. [10] have found that $FeCl_2$ pretreatment may improve P removal performance of bauxite residue, probably because its higher Fe content after $FeCl_2$ pretreatment enhances P binding to Fe compounds. Huang et al. [12] indicate that HCl pretreated bauxite residue may give P sorption capacities 2.5 times higher than raw bauxite residue. According to Huang et al. [12], HCl pretreatment neutralizes the negative charged OH^- ions on the alkaline surface of bauxite residue, thus promoting electrostatic adsorption of negatively charged phosphate ions. Most of the studies in Table 2 have found that the pseudo second order model describes P sorption kinetic better than the pseudo first order model. Yin et al. [8] have obtained R^2 values of pseudo second order model (0.9942–0.9999) higher than those of pseudo first order model (0.8827–0.9929) for all the experimental conditions, and they concluded that P sorption was mainly governed by chemical interaction rather than P adsorption. Interestingly, although the pseudo first order was not suitable, they also found that R^2 values of pseudo first order increased slightly as the initial P concentration decreased from 10 to 5 mg P/L, thus suggesting that P adsorption had a more significant impact on the effective sorption capacity at lower P concentration. However, more caution should be exercised when interpreting kinetic data by using a model equation, as a good mathematical description of experimental data is not sufficient enough to validate the underlying mechanism [27,31]. Furthermore, P saturation of bauxite residue was not reached in most studies, and it is likely that the experimental P sorption capacities at the equilibrium were more influenced by the concentrations of one or more reactants becoming limiting rather than by physical-chemical equilibria at the interface between solution and bauxite residue. Therefore, supplementary experiments and further investigation are needed to elucidate P removal mechanisms.

3.2. P sorption mechanisms in batch conditions

A series of supplementary batch experiments was performed to investigate the effect of different water composition on P removal mechanisms. For each experiment, the main physical-chemical parameters of the solutions at initial time and after 24 h of contact time, the experimental P sorption capacities after 24 h of contact time, and the modeled equilibrium P sorption capacities q_{e2} calculated by Eq. (5), are summarized in Table 3. A significant increase in Ca concentrations and pH values of the solutions was observed for all experiments after 24 h of contact time (Table 3). According to Kirwan et al. [33], these alkaline releases can be attributed to the dissolution of various compounds that

Table 2
Main results from recent batch studies that have investigated P sorption capacities of raw and modified bauxite residue: GBR = Granulated Bauxite Residue; RBR = Raw Bauxite Residue; FeMBR = $FeCl_3$ modified Bauxite Residue; TTBR = high Temperature Treated Bauxite Residue; PMBR = Polypyrrole Modified Bauxite Residue; CBR = Carbonated Bauxite Residue.

Study	Experimental parameters						Experimental results		
	Sorbent material	Size (mm)	Type of P solution	Initial P (mg P/L)	Sorbent dose (g/L)	Contact time (h)	P removal performance (%)	Experimental P sorption capacity at equilibrium (mg P/g material)	Modeled P sorption capacity at equilibrium (mg P/g material)[a]
Zhao et al. [11]	GBR	1.5	Synthetic	50	4	8	47–53	5.88–6.64	6.74–8.36
Wang et al. [10]	RBR	< 0.15	Synthetic	100	8	48	52[b]	6.5[b]	8.31
	FeMBR	< 0.15	Synthetic	100	2	48	66[b]	33[b]	33.56
Li et al. [32]	PMBR	< 0.15	Synthetic	10	0.1	0.5	2[b]	2.11	2.15
Park et al. [29]	RBR	N.A.[c]	Synthetic	100	8	24	46[b]	5.7[b]	5.55
	TTBR	N.A.[c]	Synthetic	100	8	24	> 99[b]	13.1[b]	13.21
Yin et al. [8]	PMBR	< 0.25	Synthetic	5	1	10	75–97[b]	3.75–4.85	3.96–4.96
	PMBR	< 0.25	Synthetic	10	1	10	46–88[b]	4.65–8.76	4.84–8.57
This study	CBR	< 2	Synthetic	8.3–11.1	50	6	96–98	0.16–0.21	0.17–0.22
	CBR	< 2	Synthetic	50–51.3	50	6	92–93	0.92–0.96	0.98–1.12
	CBR	< 2	Synthetic	98–104.9	50	6	86–91	1.76–1.90	2.03–2.32
	CBR	< 2	Synthetic	195.4–202.5	50	6	87–90	3.44–3.66	3.85–3.99
	CBR	< 2	Real effluent	5.9	50	6	97	0.12	0.12

[a] According to the pseudo second order kinetic model.
[b] Based on article data.
[c] Not Available data.

Table 3
Main results from supplementary batch P sorption experiments performed to investigate P removal mechanisms from aqueous solutions at different initial P concentrations: 10 H_2O = deionized water at around 10 mg P/L; 100 H_2O = deionized water at around 100 mg P/L; 10 WW = real effluent at around 10 mg P/L; 100 WW = real effluent at around 100 mg P/L.

Parameter	Test code			
	10 H_2O	10 WW	100 H_2O	100 WW
Initial P (mg P/L)	9.64	14.3	99.9	107.1
Initial Ca (mg Ca/L)	No[a]	110.1	No[a]	93.6
Initial Al (mg Al/L)	No[a]	< LD[b]	No[a]	< LD[b]
Initial Fe (mg Fe/L)	No[a]	0.06	No[a]	0.07
Initial pH (-)	6.00	8.02	5.14	6.55
P after 24 h (mg P/L)[c]	0.15 ± 0.02	0.10 ± 0.13	2.72 ± 0.13	2.01 ± 0.13
Ca after 24 h (mg Ca/L)[c]	507.0 ± 1.7	536.8 ± 10.7	433.5 ± 28.5	455.5 ± 44.8
Al after 24 h (mg Al/L)[c]	1.05 ± 0.37	0.93 ± 0.21	0.68 ± 0.97	1.96 ± 0.14
Fe after 24 h (mg Fe/L)[c]	0.53 ± 0.02	0.28 ± 0.02	0.84 ± 1.12	2.69 ± 0.11
pH after 24 h (-)[c]	8.59 ± < 0.01	8.48 ± 0.01	7.60 ± 0.01	7.64 ± 0.01
Experimental P sorption capacity after 24 h (mg P/g CBR)[c]	0.19 ± < 0.01	0.28 ± < 0.01	1.94 ± < 0.01	2.10 ± < 0.01
Modeled equilibrium P sorption capacity q_{e2} (mg P/g CBR)[d]	0.194	0.287	2.01	2.15

[a] Synthetic solution prepared with deionized water plus KH_2PO_4.
[b] Limit of detection for Al analysis (0.001 mg Al/L).
[c] Average value ± standard deviation from duplicate experiments.
[d] Calculated by Eq. (5).

are present in gypsum-treated bauxite residue, including calcite ($CaCO_3$), tri-calcium aluminate ($Ca_3Al_2(OH)_{12}$), hydrocalumite ($Ca_3Al_2(OH)_{12}CaCO_3$•5 H_2O), and others calcium aluminates, as shown by the dissociation Eqs. (6)–(8), respectively[33–35].

$$CaCO_3 \leftrightarrow Ca^{2+} + CO_3^{2-} \quad (6)$$

$$Ca_3Al_2(OH)_{12} \leftrightarrow 3Ca^{2+} + 4OH^- + 2Al(OH)_4^- \quad (7)$$

$$Ca_3Al_2(OH)_{12}\bullet CaCO_3\bullet 5H_2O \leftrightarrow 4Ca^{2+} + 4OH^- + 2Al(OH)_4^- + CO_3^{2-} + 5H_2O \quad (8)$$

Complementary leaching tests performed according to EN 12457–2 (2002) have indicated that the equilibrium pH of CBR leachate is 8.50 ± 0.01 (average value ± standard deviation of duplicate experiments). This pH value is much lower than the common pH values of leachates from untreated bauxite residue (10−13) [1]. Several studies in the literature have already found that gypsum-treated bauxite residue at 5–8% mass ratios (mass of gypsum to mass of bauxite residue) can reduce the pH of CBR leachates to values of 8–9 [19,33–35]. This was primarily attributed to the precipitation of soluble alkali compounds (e.g. NaOH, Na_2CO_3, $NaHCO_3$, $NaAl(OH)_4$, KOH, K_2CO_3)[34] to more stable calcite, tri-calcium aluminate, hydrocalumite, and other calcium aluminate minerals during the treatment with gypsum [33,35–38], which exhibit lower solubility and therefore give lower alkaline release. As shown in Table 3, the difference between modeled equilibrium P sorption capacities q_{e2} and experimental P sorption capacities after 24 h of contact time is always lower than 3.5%, thus suggesting that a pseudo equilibrium in P sorption was achieved for all experiments.

Fig. 3 summarizes the results of P sequential extractions from raw CBR and from CBR after P sorption experiments. As shown in Fig. 3, P amounts extracted in step AI-P were more than 10 times higher than those extracted in step NAI-P for all the experiments, thus indicating that apatite P predominated over the non-apatite P form in all samples. The total amount of P extracted from raw CBR was 0.91 ± 0.01 mg P/g CBR, whereas the total amounts of P extracted from CBR after batch

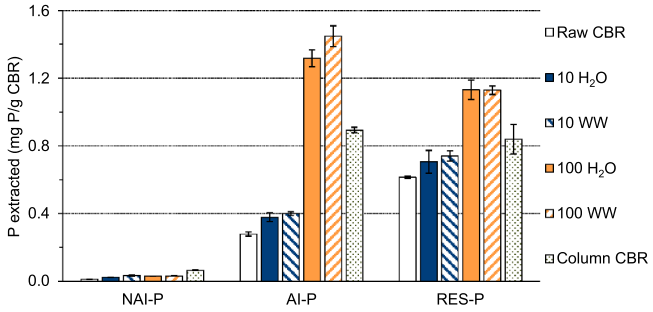

Fig. 3. Results of P sequential extractions from raw CBR, from CBR after batch P sorption experiments (tests 10 H_2O, 10 WW, 100 H_2O, and 100 WW), and from CBR taken from a column after 140 days of continuous flow P sorption experiments [25] (Column CBR). Average values from duplicate experiments, bars indicating the range min-max values.

experiments were 1.11 ± 0.06, 1.18 ± 0.06, 2.48 ± 0.15, and 2.61 ± 0.12 mg P/g CBR for test 10 H_2O, 10 WW, 100 H_2O, and 100 WW, respectively. The differences between the total amounts of P extracted from CBR after batch experiments and the total amount of P extracted from raw CBR give about 0.20, 0.27, 1.57, and 1.70 mg P/g CBR for test 10 H_2O, 10 WW, 100 H_2O, and 100 WW, respectively. These values are close to those of the experimental P sorption capacities (Table 3), indicating P recovery mass balances of about 95%, 96%, 81%, and 81% for test 10 H_2O, 10 WW, 100 H_2O, and 100 WW, respectively. The lacks in mass balance can be attributed to P losses during sequential extractions and/or P sorbed in very stable forms that were recalcitrant to extraction, especially for tests performed at higher initial P concentrations (100 H_2O and 100 WW).

As shown in Fig. 4A, the main P fraction in raw CBR is RES-P (67.9%), followed by AI-P (30.8%), and NAI-P (1.3%). After batch experiments, a change on P distribution between RES-P, AI-P, and NAI-P fractions was observed for all experiments compared to raw CBR. Overall, no significant effect on P fractionation was observed when using deionized water or real effluent as aqueous matrix, whereas initial P concentration appears to be the main parameter influencing P fractionation of CBR (Fig. 4). On the one hand, when using lower initial P concentrations (test 10 H_2O and 10 WW) NAI-P fraction increased from 1.3% (raw CBR) to 2.1% (10 H_2O) and to 2.9% (10 WW), whereas AI-P fraction increased from 30.8% (raw CBR) to 34.2% (10 H_2O) and to 34.1% (10 WW). This suggests that P sorption at lower initial P concentration was due to a mix of removal mechanisms, probably including phosphate adsorption on CBR surface, P binding to Al and/or Fe complexes, and chemical precipitation of Ca phosphates. On the other hand, when using higher initial P concentrations (test 100 H_2O and 100 WW) no significant increase on NAI-P fraction of CBR was observed after batch experiments, whereas AI-P fraction increased from 30.8% (raw CBR) to 53.1% (100 H_2O) and to 55.5% (100 WW). This suggests that Ca phosphate precipitation was the most relevant P removal mechanism at higher P concentration. The lower Ca concentrations at the end of test 100 H_2O and 100 WW (433.5 ± 28.5 and 455.5 ± 44.8 mg Ca/L, respectively) compared to test 10 H_2O and 10 WW (507.0 ± 1.7 and 536.8 ± 10.7 mg Ca/L, respectively) (Table 3) appear to confirm higher Ca consumption for Ca phosphate precipitation at higher initial P concentration.

Table 4 summarizes P, Ca, Al, and Fe extraction capacities (mg element/g CBR) obtained by sequential extractions from raw CBR and from CBR after P sorption experiments. For all experiments, Fe concentrations of the NAI-P extracts were lower than the limit of detection (0.01 mg Fe/L), thus suggesting that P extracted in this step was not related to dissolution of Fe-P complexes. This appears to be in good agreement with the results of previous experiments [25] which have indicated that over 98% of the total Fe (hydro)-oxides contained in the CBR are in the more stable crystalline form, and therefore they are

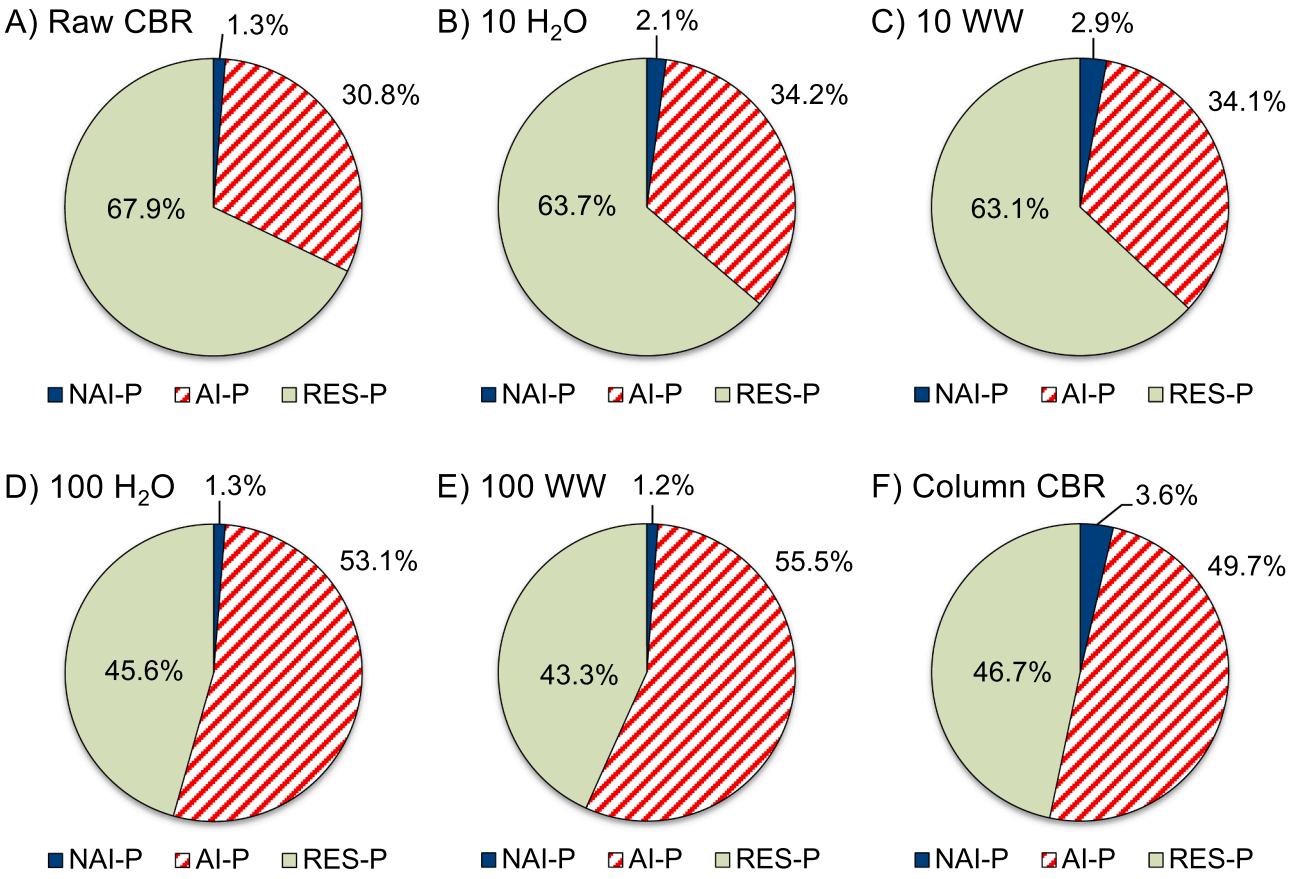

Fig. 4. P fractionations of raw CBR (A), CBR after batch P sorption experiments 10 H_2O (B), 10 WW (C), 100 H_2O (D), and 100 WW (E), and CBR taken from a column after 140 days of continuous flow P sorption experiments [25] (F).

Table 4
Elemental P, Ca, Al, and Fe extraction capacities obtained by sequential extraction experiments from raw and used CBR samples (average values ± standard deviations from duplicate experiments): raw CBR samples, CBR samples after batch P sorption experiments 10 H_2O, 10 WW, 100 H_2O, and 100 WW, and CBR samples taken from a column after 140 days of continuous flow P sorption experiments [25].

Extraction step	Element	Test code					
		Raw CBR	10 H_2O	10 WW	100 H_2O	100 WW	Column CBR
Element extracted at Step 1: NAI-P (mg element /g CBR)	P	0.012 ± 0.001	0.023 ± 0.001	0.034 ± 0.006	0.031 ± 0.001	0.031 ± 0.006	0.064 ± 0.002
	Ca	0.560 ± 0.030	0.255 ± 0.021	0.254 ± 0.009	0.170 ± 0.002	0.210 ± 0.054	0.166 ± 0.035
	Al	1.92 ± 0.26	1.91 ± 0.01	1.97 ± 0.02	2.35 ± 0.01	2.16 ± 0.28	3.15 ± 0.15
	Fe	< LD[a]	< LD[a]	< LD[a]	< LD[a]	< LD[a]	< LD[a]
Element extracted at Step 2: AI-P (mg element /g CBR)	P	0.28 ± 0.02	0.38 ± 0.04	0.40 ± 0.02	1.32 ± 0.07	1.45 ± 0.09	0.89 ± 0.02
	Ca	42.2 ± 0.5	32.1 ± 0.8	33.3 ± 0.5	32.6 ± 0.7	35.0 ± 0.6	38.0 ± 0.5
	Al	22.6 ± 0.2	20.5 ± 0.2	20.7 ± 0.2	20.0 ± 0.4	20.8 ± 0.2	17.3 ± 1.3
	Fe	2.12 ± 0.09	2.01 ± 0.03	1.96 ± 0.09	1.70 ± 0.03	1.74 ± < 0.01	1.83 ± 0.01
Element extracted at Step 3: RES-P (mg element/g CBR)	P	0.62 ± 0.01	0.71 ± 0.09	0.74 ± 0.04	1.13 ± 0.08	1.13 ± 0.03	0.84 ± 0.12
	Ca	2.34 ± 0.40	2.20 ± 0.01	2.12 ± 0.16	2.57 ± 0.09	2.50 ± 0.08	2.18 ± 0.36
	Al	8.99 ± 0.96	8.38 ± 0.68	8.32 ± 0.50	7.56 ± 0.42	8.18 ± 0.91	7.70 ± 0.48
	Fe	191.3 ± 11.9	190.0 ± 11.7	182.9 ± 2.5	186.2 ± 7.2	185.7 ± 8.2	174.7 ± 20.3
Total element extracted (mg element/g CBR)	P	0.91 ± 0.01	1.11 ± 0.06	1.18 ± 0.06	2.48 ± 0.15	2.61 ± 0.12	1.80 ± 0.15
	Ca	45.1 ± 0.9	34.6 ± 0.8	35.7 ± 0.3	35.3 ± 0.6	37.8 ± 0.7	40.4 ± 0.1
	Al	33.5 ± 0.7	30.8 ± 0.9	31.0 ± 0.7	29.9 ± 0.8	31.2 ± 1.2	28.1 ± 1.0
	Fe	193.4 ± 11.9	192.0 ± 11.7	184.8 ± 2.4	187.9 ± 7.2	187.5 ± 8.2	176.5 ± 20.3

[a] Limit of detection for Fe analysis (0.01 mg Fe/L).

poorly mobilizable for Fe-P precipitation. Differently from Fe, Al concentrations of NAI-P extracts were not negligible thus giving Al extraction capacities ranging from a minimum of 1.91 ± 0.01 to a maximum of 2.35 ± 0.01 mg Al/g CBR for test 10 H_2O and 100 H_2O, respectively. However, no direct relationship between Al and P extraction was found, as the molar ratios between Al and P extracted in step NAI-P varied from 67.8 to 87.0, 91.4, and 94.6 for test 10 WW, 100 H_2O, 100 WW, and 10 H_2O, respectively. Moreover, these experimental molar ratios are several orders of magnitude higher than the theoretical molar ratio of the most common Al-P precipitate in water systems ($AlPO_4$). Most probably, these Al extracts in step NAI-P are due to the dissociation of calcium aluminates in NaOH solution, according to Eq. (9), as described by Azof et al. [39].

$$Ca_3Al_2(OH)_{12} + 2Na^+ + 2OH^- \leftrightarrow 3Ca^{2+} + 2Na^+ + 6OH^- + 2Al(OH)_4^- \quad (9)$$

It should also be noticed in Table 4 that NAI-P rises from 0.012

± 0.001 mg P/g CBR for raw CBR to stabilize at around 0.032 mg P/g CBR for test 10 WW, 100 H_2O, and 100 WW, thus suggesting saturation of the adsorption sites. According to these results, it is likely that P extraction in step NAI-P was mainly due to desorption of phosphates that were adsorbed on the CBR surface [16], including P bound to Al and/or Fe (hydro)-oxides, and that were desorbed at high pH by OH^- ligand exchange, as proposed in Eqs. (10)–(12) (adapted from Li et al. [40]), where S represent the CBR surface.

$$S\text{-}H_2PO_4 + OH^- \rightarrow S\text{-}OH + H_2PO_4^- \quad (10)$$

$$S\text{-}HPO_4 + 2(OH^-) \rightarrow S\text{-}(OH)_2 + HPO_4^{2-} \quad (11)$$

$$S\text{-}PO_4 + 3(OH^-) \rightarrow S\text{-}(OH)_3 + PO_4^{3-} \quad (12)$$

Instead, AI-P rises from 0.28 ± 0.02 mg P/g CBR for raw CBR to 0.38 ± 0.04, 0.40 ± 0.02, 1.32 ± 0.07, and 1.45 ± 0.09 mg P/g CBR for test 10 H_2O, 10 WW, 100 H_2O, and 100 WW, respectively. Moreover, AI-P fraction of CBR after P sorption experiments shows the highest relative increase compared to raw CBR. These results appear to confirm that Ca phosphate precipitation was the most relevant P removal mechanism for all experiments, especially at higher initial P concentration (test 100 H_2O and 100 WW), and that Ca phosphate precipitation does not depend on the availability of adsorption sites, and it may occur regardless of the saturation of the adsorption sites. The molar ratio between Ca and P extracted in step AI-P varied from 18.7 (test 100 WW) to 65.8 (test 10 H_2O), which are several orders of magnitude higher than the molar ratios of the most common Ca-P compounds (1–1.67) [41]. Probably, $CaCO_3$ dissolution from CBR during AI-P extraction at low pH may explain the molar ratios between extracted Ca to extracted P higher than the theoretical Ca/P molar ratios of Ca-P compounds. As shown in Table 4, RES-P rises from 0.62 ± 0.01 mg P/g CBR for raw CBR to 0.71 ± 0.09, 0.74 ± 0.04, 1.13 ± 0.08, and 1.13 ± 0.03 mg P/g CBR for test 10 H_2O, 10 WW, 100 H_2O, and 100 WW, respectively, thus indicating a more significant increase for tests performed at higher initial P concentration (100 H_2O and 100 WW). According to several authors, RES-P can be attributed to P in very stable compounds that are recalcitrant to 1 M HCl extraction [42,43]. It is likely that the increase in RES-P content of CBR after P sorption is primarily related to precipitation of hydroxyapatite crystals (HAP) according to Eq. (13) [44], as HAP represents the most thermodynamically stable form of Ca phosphate in wastewater systems [41].

$$5Ca^{2+} + 3PO_4^{3-} + OH^- \rightarrow Ca_5(PO_4)_3(OH) \quad (13)$$

This hypothesis is supported by the lower pH values at the end of test 100 H_2O and 100 WW (7.6 and 7.64, respectively) compared to those of test 10 H_2O and 10 WW (8.59 and 8.48, respectively), which suggest higher OH^- consumption for HAP precipitation at higher initial P concentration, according to Eq. (13).

The total amounts of Ca, Al, and Fe extracted from raw CBR are 45.1 ± 0.9, 33.5 ± 0.7, and 193.4 ± 11.9 mg/g CBR, respectively, and their values are higher than those extracted from CBR after batch experiments. These results appears to confirm Ca, Al, and Fe releases from CBR when it is put in contact with water, as described in previous studies [18,45], with Ca the most leachable element among Ca, Al, and Fe.

Overall, results of this study suggest two main types of P removal mechanisms occurring in batch experiments.

1. Phosphate adsorption on CBR surface. This first type of P removal mechanism depends closely on the availability of the adsorption sites on the CBR surface, with a maximum adsorption capacity of approximately 0.03 mg P/g CBR.
2. Precipitation of Ca phosphates. This second type of P removal mechanism is likely to be composed of two consecutive reactive phases. First, alkaline release from CBR produces an increase in the concentrations of Ca^{2+} and OH^- ions in the solutions. Then, higher Ca^{2+} concentrations and high pH values promote Ca phosphate precipitation, as it is well known from the literature that the solubility of the most common Ca phosphates in wastewater systems decreases strongly as the pH rises above 8 [46].

3.3. P sorption mechanisms in continuous flow conditions

The sequential P extraction procedure described in Section 2.3 was also applied to CBR samples (Column CBR) taken from a column after 140 days of continuous flow P sorption experiments. The column was operated under aerobic conditions and according to a theoretical hydraulic retention time based on the initial void volume (HRTv) of around 24 h. During the first 54 days of operation, the column was fed with a synthetic solution of about 10 mg P/L and 40 mg N-NO_3/L (prepared with tap water, KH_2PO_4, and KNO_3). Then, from day 55–140, the column was fed with the real effluent from a small WWTP (Rougiers, France, main physical-chemical parameters in Table S1). Complete details on design and performances of column experiments are available in Barca et al. [25]. The total amount of P extracted from Column CBR was 1.80 ± 0.15 mg P/g CBR (Table 4), and the main P fractions were AI-P (49.7%), RES-P (46.7%), and NAI-P (3.6%), with AI-P showing the highest relative increase compared to raw CBR (Fig. 4F). This confirms that Ca phosphate precipitation was the main P removal mechanism in continuous flow experiments. However, it should be noticed that NAI-P in Column CBR (0.064 ± 0.002 mg P/g CBR) was 1.9–2.8 times higher than those of CBR after batch experiments (Table 4). This suggests a higher potential for P removal by phosphate adsorption under continuous flow rather than batch conditions. Most likely, the long duration of the column experiments (140 days) had favored a more efficient intra-particle diffusion of wastewater inside the CBR, thus improving the contact between wastewater and adsorption sites. The results from previous column experiments have also indicated that different aeration conditions and organic content of the feed can affect P removal mechanisms in CBR columns [25]. Indeed, it was found that under anoxic conditions and in the presence of organic carbon (glucose), microbially driven mobilization of Fe from CBR can provide Fe ions for further Fe-P precipitation, but also it may lead to Fe release from the CBR filters.

4. Conclusions

The results of this study confirm that CBR is an efficient sorbent material for P removal from wastewater. The initial P concentration appears to be the most influential parameter affecting kinetics, capacities, and mechanisms of P sorption in batch experiments. Kinetic constants of P sorption increased exponentially with decreasing initial P concentration below 100 mg P/L, thus indicating a faster achievement of P sorption equilibrium. P sorption capacities at equilibrium increased linearly from about 0.2 to about 3.9 mg P/g CBR with increasing initial P concentration from about 10 to about 200 mg P/L, thus indicating that P saturation of CBR was not reached. Precipitation of Ca phosphates appears to be the main P removal mechanism for all experiments, especially at higher initial P concentrations (100 mg P/L), whereas phosphate adsorption on CBR surface appears to be more relevant over the total amount of P removed when treating solutions at lower P concentrations (10 mg P/L). Batch experiments also indicate that maximum adsorption capacities on CBR surface is approximately 0.03 mg P/g CBR, and Ca P precipitation may occur regardless of the saturation of the adsorption sites, thus increasing the actual P sorption capacities.

CRediT authorship contribution statement

Cristian Barca: Conceptualization, Investigation, Writing – original draft, Visualization, Project administration, Funding acquisition. **Matteo Magari:** Investigation. **Hélène Miche**: Investigation. **Pierre Hennebert:** Validation, Writing – review & editing, Supervision.

Declaration of Competing Interest

The authors declare that they have no known competing financial interests or personal relationships that could have appeared to influence the work reported in this paper.

Data availability

Data will be made available on request.

Acknowledgments

This work was funded by the Labex DRIIHM, French program "Investissements d'Avenir" (ANR-11-LABX-0010) which is managed by the ANR. We thank Laurent Poizat (ALTEO) for providing CBR samples.

Appendix A. Supplementary material

Supplementary data associated with this article can be found in the online version at doi:10.1016/j.jece.2022.108922.

References

[1] F. Lyu, Y. Hu, L. Wang, W. Sun, Dealkalization processes of bauxite residue: a comprehensive review, J. Hazard. Mater. 403 (2021), 123671, https://doi.org/10.1016/j.jhazmat.2020.123671.
[2] É. Ujaczki, V. Feigl, M. Molnár, P. Cusack, T. Curtin, R. Courtney, L. O'Donoghue, P. Davris, C. Hugi, M.W. Evangelou, E. Balomenos, M. Lenz, Re-using bauxite residues: benefits beyond (critical raw) material recovery, J. Chem. Technol. Biotechnol. 93 (2018) 2498–2510, https://doi.org/10.1002/jctb.5687.
[3] K. Evans, The history, challenges, and new developments in the management and use of bauxite residue, J. Sustain. Metall. 2 (2016) 316–331, https://doi.org/10.1007/s40831-016-0060-x.
[4] M. Wang, X. Liu, Applications of red mud as an environmental remediation material: a review, J. Hazard. Mater. 408 (2021), 124420, https://doi.org/10.1016/j.jhazmat.2020.124420.
[5] M.A. Grace, M.G. Healy, E. Clifford, Use of industrial by-products and natural media to adsorb nutrients, metals and organic carbon from drinking water, Sci. Total Environ. 518–519 (2015) 491–497, https://doi.org/10.1016/j.scitotenv.2015.02.075.
[6] A. Hu, G. Ren, J. Che, Y. Guo, J. Ye, S. Zhou, Phosphate recovery with granular acid-activated neutralized red mud: fixed-bed column performance and breakthrough curve modelling, J. Environ. Sci. 90 (2020) 78–86, https://doi.org/10.1016/j.jes.2019.10.018.
[7] R.A. Pepper, S.J. Couperthwaite, G.J. Millar, Re-use of waste red mud: production of a functional iron oxide adsorbent for removal of phosphorous, J. Water Process Eng. 25 (2018) 138–148, https://doi.org/10.1016/j.jwpe.2018.07.006.
[8] Y. Yin, G. Xu, Y. Xu, M. Guo, Y. Xiao, T. Ma, C. Liu, Adsorption of inorganic and organic phosphorus onto polypyrrole modified red mud: evidence from batch and column experiments, Chemosphere 286 (2022), 131862, https://doi.org/10.1016/j.chemosphere.2021.131862.
[9] J.T. Bunce, E. Ndam, I.D. Ofiteru, A. Moore, D.W. Graham, A review of phosphorus removal technologies and their applicability to small-scale domestic wastewater treatment systems, Front. Environ. Sci. 6 (2018), https://doi.org/10.3389/fenvs.2018.00008.
[10] Y. Wang, Y. Yu, H. Li, C. Shen, Comparison study of phosphorus adsorption on different waste solids: Fly ash, red mud and ferric–alum water treatment residues, J. Environ. Sci. 50 (2016) 79–86, https://doi.org/10.1016/j.jes.2016.04.025.
[11] Y. Zhao, Q. Yue, Q. Li, X. Xu, Z. Yang, X. Wang, B. Gao, H. Yu, Characterization of red mud granular adsorbent (RMGA) and its performance on phosphate removal from aqueous solution, Chem. Eng. J. 193–194 (2012) 161–168, https://doi.org/10.1016/j.cej.2012.04.040.
[12] W. Huang, S. Wang, Z. Zhu, L. Li, X. Yao, V. Rudolph, F. Haghseresht, Phosphate removal from wastewater using red mud, J. Hazard. Mater. 158 (2008) 35–42, https://doi.org/10.1016/j.jhazmat.2008.01.061.
[13] J.-Y. Lin, M. Kim, D. Li, H. Kim, C. Huang, The removal of phosphate by thermally treated red mud from water: the effect of surface chemistry on phosphate immobilization, Chemosphere 247 (2020), 125867, https://doi.org/10.1016/j.chemosphere.2020.125867.
[14] Y. Zhao, Q. Yue, Q. Li, Q. Li, B. Gao, S. Han, H. Yu, Influence of sintering temperature on orthophosphate and pyrophosphate removal behaviors of red mud granular adsorbents (RMGA), Colloids Surf. A Physicochem. Eng. Asp. 394 (2012) 1–7, https://doi.org/10.1016/j.colsurfa.2011.11.013.
[15] S. Wang, H. Ang, M. Tade, Novel applications of red mud as coagulant, adsorbent and catalyst for environmentally benign processes, Chemosphere 72 (2008) 1621–1635.
[16] R. Liu, L. Chi, X. Wang, Y. Sui, Y. Wang, H. Arandiyan, Review of metal (hydr)oxide and other adsorptive materials for phosphate removal from water, J. Environ. Chem. Eng. 6 (2018) 5269–5286, https://doi.org/10.1016/j.jece.2018.08.008.
[17] L.M. Despland, M.W. Clark, T. Vancov, D. Erler, M. Aragno, Nutrient and trace-metal removal by bauxsol pellets in wastewater treatment, Environ. Sci. Technol. 45 (2011) 5746–5753, https://doi.org/10.1021/es200934y.
[18] P.B. Cusack, O. Callery, R. Courtney, É. Ujaczki, L.M.T. O'Donoghue, M.G. Healy, The use of rapid, small-scale column tests to determine the efficiency of bauxite residue as a low-cost adsorbent in the removal of dissolved reactive phosphorus from agricultural waters, J. Environ. Manag. 241 (2019) 273–283, https://doi.org/10.1016/j.jenvman.2019.04.042.
[19] P.B. Cusack, M.G. Healy, P.C. Ryan, I.T. Burke, L.M.T. O' Donoghue, É. Ujaczki, R. Courtney, Enhancement of bauxite residue as a low-cost adsorbent for phosphorus in aqueous solution, using seawater and gypsum treatments, J. Clean. Prod. 179 (2018) 217–224, https://doi.org/10.1016/j.jclepro.2018.01.092.
[20] J. Paing, A. Guilbert, V. Gagnon, F. Chazarenc, Effect of climate, wastewater composition, loading rates, system age and design on performances of French vertical flow constructed wetlands: a survey based on 169 full scale systems, Ecol. Eng. 80 (2015) 46–52, https://doi.org/10.1016/j.ecoleng.2014.10.029.
[21] Y.S. Ho, G. McKay, A comparison of chemisorption kinetic models applied to pollutant removal on various sorbents, Process Saf. Environ. Prot. 76 (1998) 332–340, https://doi.org/10.1205/095758298529696.
[22] J.J. González Medeiros, B. Pérez Cid, E. Fernández Gómez, Analytical phosphorus fractionation in sewage sludge and sediment samples, Anal. Bioanal. Chem. 381 (2005) 873–878, https://doi.org/10.1007/s00216-004-2989-z.
[23] M.J. Hedley, J.W.B. Stewart, B.S. Chauhan, Changes in inorganic and organic soil phosphorus fractions induced by cultivation practices and by laboratory incubations, Soil Sci. Soc. Am. J. 46 (1982) 970–976, https://doi.org/10.2136/sssaj1982.03615995004600050017x.
[24] H. Tiessen, J.O. Moir, Characterization of available P by sequential extraction, Soil Sampl. Methods Anal. 7 (1993) 5–229.
[25] C. Barca, D. Scanu, N. Podda, H. Miche, L. Poizat, P. Hennebert, Phosphorus removal from wastewater by carbonated bauxite residue under aerobic and anoxic conditions, J. Water Process Eng. (2020), 101757, https://doi.org/10.1016/j.jwpe.2020.101757.
[26] J. Bujdák, Adsorption kinetics models in clay systems. The critical analysis of pseudo-second order mechanism, Appl. Clay Sci. 191 (2020), 105630, https://doi.org/10.1016/j.clay.2020.105630.
[27] J.-P. Simonin, On the comparison of pseudo-first order and pseudo-second order rate laws in the modeling of adsorption kinetics, Chem. Eng. J. 300 (2016) 254–263, https://doi.org/10.1016/j.cej.2016.04.079.
[28] Y. Hu, C. Pan, X. Zheng, F. Hu, L. Xu, G. Xu, Y. Jian, X. Peng, Prediction and optimization of adsorption properties for Cs on NiSiO@NiAlFe LDHs hollow spheres from aqueous solution: kinetics, isotherms, and BBD model, J. Hazard. Mater. 401 (2021), 123374, https://doi.org/10.1016/j.jhazmat.2020.123374.
[29] J.-H. Park, J.J. Wang, D.-C. Seo, Sorption characteristics of phosphate by bauxite residue in aqueous solution, Colloids Surf. A Physicochem. Eng. Asp. 618 (2021), 126465, https://doi.org/10.1016/j.colsurfa.2021.126465.
[30] F.M. Kaußen, B. Friedrich, Phase characterization and thermochemical simulation of (landfilled) bauxite residue ("red mud") in different alkaline processes optimized for aluminum recovery, Hydrometallurgy 176 (2018) 49–61, https://doi.org/10.1016/j.hydromet.2018.01.006.
[31] E.C. Lima, F. Sher, A. Guleria, M.R. Saeb, I. Anastopoulos, H.N. Tran, A. Hosseini-Bandegharaei, Is one performing the treatment data of adsorption kinetics correctly? J. Environ. Chem. Eng. 9 (2021), 104813 https://doi.org/10.1016/j.jece.2020.104813.
[32] X. Li, M. Ji, L.D. Nghiem, Y. Zhao, D. Liu, Y. Yang, Q. Wang, Q.T. Trinh, D.-V.N. Vo, V.Q. Pham, N.H. Tran, A novel red mud adsorbent for phosphorus and diclofenac removal from wastewater, J. Mol. Liq. 303 (2020), 112286, https://doi.org/10.1016/j.molliq.2019.112286.
[33] L.J. Kirwan, A. Hartshorn, J.B. McMonagle, L. Fleming, D. Funnell, Chemistry of bauxite residue neutralisation and aspects to implementation, Int. J. Miner. Process. 119 (2013) 40–50, https://doi.org/10.1016/j.minpro.2013.01.001.
[34] S. Xue, M. Li, J. Jiang, G.J. Millar, C. Li, X. Kong, Phosphogypsum stabilization of bauxite residue: conversion of its alkaline characteristics, J. Environ. Sci. (2018), https://doi.org/10.1016/j.jes.2018.05.016.
[35] M. Gräfe, G. Power, C. Klauber, Bauxite residue issues: III. Alkalinity and associated chemistry, Hydrometallurgy 108 (2011) 60–79, https://doi.org/10.1016/j.hydromet.2011.02.004.
[36] Y. Wu, X. Li, J. Jiang, H. William, F. Zhu, S. Xue, Integrating column leaching experiments and geochemical modelling to predict the long-term alkaline stability during erosion process for gypsum amended bauxite residue, J. Environ. Manag. 289 (2021), 112479, https://doi.org/10.1016/j.jenvman.2021.112479.
[37] Y. Jiang, X. Qin, F. Zhu, Y. Zhang, X. Zhang, W. Hartley, S. Xue, Halving gypsum dose by Penicillium oxalicum on alkaline neutralization and microbial community reconstruction in bauxite residue, Chem. Eng. J. 451 (2023), 139008, https://doi.org/10.1016/j.cej.2022.139008.
[38] I.T. Burke, C.L. Peacock, C.L. Lockwood, D.I. Stewart, R.J.G. Mortimer, M.B. Ward, P. Renforth, K. Gruiz, W.M. Mayes, Behavior of aluminum, arsenic, and vanadium during the neutralization of red mud leachate by HCl, gypsum, or seawater, Environ. Sci. Technol. 47 (2013) 6527–6535, https://doi.org/10.1021/es4010834.
[39] F.I. Azof, Y. Yang, D. Panias, L. Kolbeinsen, J. Safarian, Leaching characteristics and mechanism of the synthetic calcium-aluminate slags for alumina recovery, Hydrometallurgy 185 (2019) 273–290, https://doi.org/10.1016/j.hydromet.2019.03.006.
[40] Y. Li, C. Liu, Z. Luan, X. Peng, C. Zhu, Z. Chen, Z. Zhang, J. Fan, Z. Jia, Phosphate removal from aqueous solutions using raw and activated red mud and fly ash, J. Hazard. Mater. 137 (2006) 374–383, https://doi.org/10.1016/j.jhazmat.2006.02.011.

[41] E. Valsami-Jones, Mineralogical controls on phosphorus recovery from wastewaters, Mineral. Mag. 65 (2001) 611–620, https://doi.org/10.1180/002646101317018433.
[42] L.M. Condron, S. Newman, Revisiting the fundamentals of phosphorus fractionation of sediments and soils, J. Soils Sediments 11 (2011) 830–840, https://doi.org/10.1007/s11368-011-0363-2.
[43] C. Gu, T. Dam, S.C. Hart, B.L. Turner, O.A. Chadwick, A.A. Berhe, Y. Hu, M. Zhu, Quantifying uncertainties in sequential chemical extraction of soil phosphorus using XANES spectroscopy, Environ. Sci. Technol. 54 (2020) 2257–2267, https://doi.org/10.1021/acs.est.9b05278.
[44] C. Barca, C. Gérente, D. Meyer, F. Chazarenc, Y. Andrès, Phosphate removal from synthetic and real wastewater using steel slags produced in Europe, Water Res. 46 (2012) 2376–2384, https://doi.org/10.1016/j.watres.2012.02.012.
[45] P. Gupta, S.J. Couperthwaite, T.C. Santini, R.A. Pepper, G.J. Millar, Experimental and geochemical modelling investigations on the weathering behaviour of bauxite residue: effect of pH, J. Environ. Chem. Eng. 9 (2021), 103509, https://doi.org/10.1016/j.jece.2019.103509.
[46] W. Stumm, J.J. Morgan, Aquatic Chemistry: Chemical Equilibria and Rates in Natural Waters, John Wiley & Sons, 2012.